Electronic Supporting Information for

Multifunctional PEGylated Magnetic Nanoclusters for Biomedical Application

Erwin Peng, Eugene Shi Guang Choo, Cherie Tan Shi Hua, Xiaosheng Tang, Yang Sheng and Junmin Xue*

Department of Materials Science and Engineering, Faculty of Engineering, National University of Singapore (NUS), 7 Engineering Drive 1, Singapore 117574.

* Email: msexuejm@nus.edu.sg

S1. TEM Size Distributions, XRD and VSM of Various MFNPs

The size distributions of MFNPs were obtained from the direct measurements of 100-200 MFNPs from the TEM images. The size of MFNPs were determined as the nanocrystals diameter for the spherically shaped MFNPs and the nanocrystals tip-to-tip length for the octahedral shaped MFNPs. 4 different sizes of MFNPs were successfully synthesized from the thermal decomposition method, namely MFNPs-A, MFNPs-B, MFNPs-C and MFNPs-D with an average size of 5.66 ± 0.41 nm, 10.63 ± 1.02 nm, 13.53 ± 0.99 nm and 18.17 ± 1.58 nm for respective samples. The TEM size distributions for all MFNPs are given in **Fig. S1**.

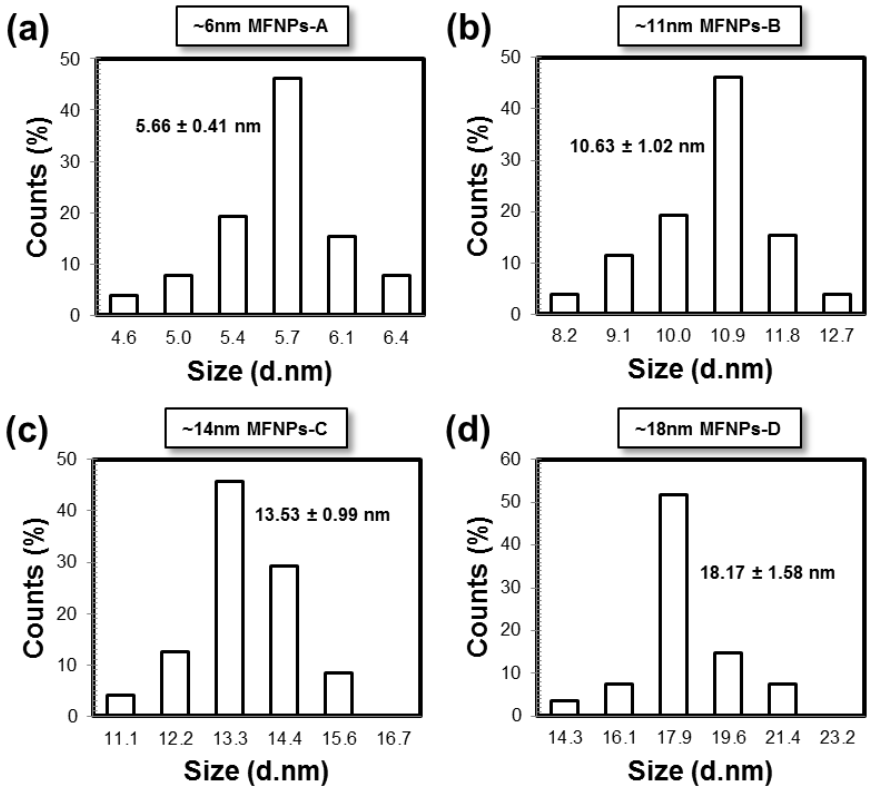

Fig. S1 TEM size distributions of: (a) MFNPs-A (~6 nm), (b) MFNPs-B (~11nm), (c) MFNPs-C (~14nm) and (d) MFNPs-D (~18nm).

The as-synthesized MFNPs samples crystallinity was analyzed using powder x-ray diffractometer. The XRD patterns of various MFNPs shown in **Fig. S2a** revealed the characteristic peaks for the typical manganese ferrite, $MnFe_2O_4$ (Jacobsite). The characteristic peaks at around 30.2^o, 35.6^o, 43.2^o, 53.0^o and 62.8^o correspond to (220), (311), (400), (422),

(333) and (440) diffraction planes. The XRD patterns of MFNPs A-D showed peak broadening from MFNPs-D to MFNPs-A which was caused by the nano-crystallite size effects. Overall, the XRD patterns suggested that MFNPs A-D exhibited high degree of crystallinity.

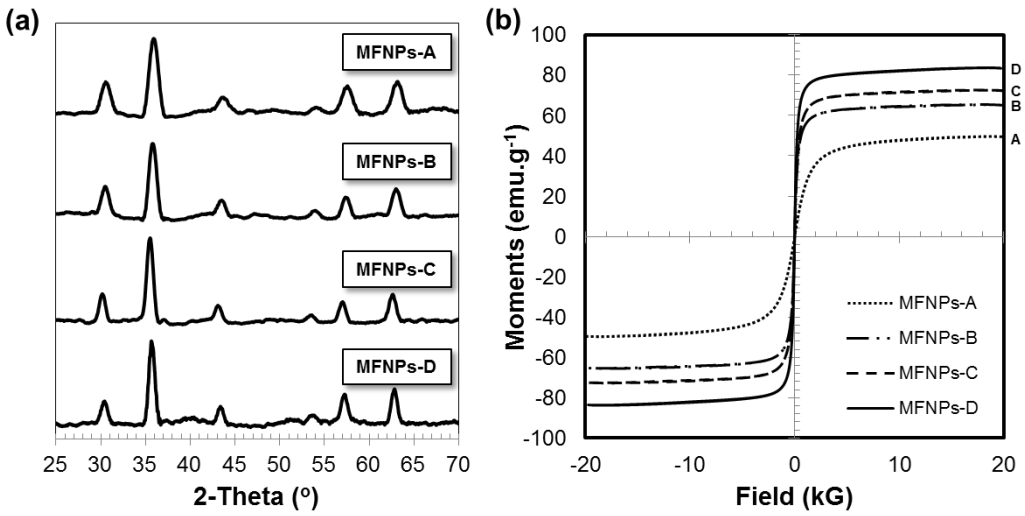

Fig. S2 (a) XRD pattern of various MFNPs recorded at 300K. (b) Hysteresis loop of various MFNPs samples measured by VSM experiment at 300K.

The hysteresis loop of MFNPs A-D samples were measured through vibrating sample magnetometry (VSM) at 300K and shown in **Fig. S2b**. The hysteresis loop of MFNPs A-D showed superparamagnetism properties in which no magnetic remnant (M_R) was observed with almost negligible coercive field (H_C). The saturation magnetization (M_S) values of MFNPs samples were found to be 49.5, 65.1, 72.3 and 83.4 emu.g^{-1} for MFNPs-A, MFNPs-B, MFNPs-C and MFNPs-D respectively. Overall, as the size of MFNPs decreases (from MFNPs-D to MFNPs-A), the overall M_S value decreases due to more surface area (per volume) and surface defects.

S2. VSM and DLS results of MFNPs/PMAO Magnetic Nanoclusters

Formation of MFNCs: Preliminary Study Using PMAO

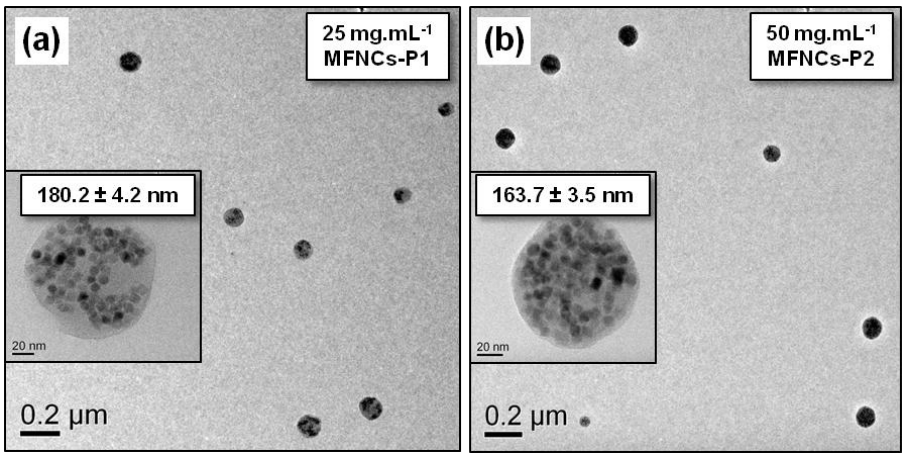

Fig. S3 TEM images of PMAO-coated magnetic nanoclusters samples with different MFNPs-2 loading represented by the MFNPs/PMAO ratio: (a) 1.25:1 (MFNCs-P1), (b) 2.5:1 (MFNCs-P2). Insets: higher magnification TEM images of the respective single nanoclusters.

In order prepare such hydrophobic nanoparticles for various biomedical applications; phase transfer (or water solubilisation) process to render the nanoparticles hydrophilic typically is required. Up to date, various amphiphilic brush co-polymers that have both hydrophobic and hydrophilic segments have been well studied in the literature, especially as a host to encapsulate hydrophobic nanocrystals. Such polymers include polystyrene/polyacrylic acid block copoylmers (PS-*b*-PAA), polyacrylic acid/P123 block copolymers (PAA-*b*-P123), poly (isobutylene-*alt*-maleic anhydride) grafted with dodecylamine (PBMA-*g*-C_{12}), poly (maleic anhydride-*alt*-1-octadecene) (PMAO), carboxylated pluronic (F127-COOH) and etc. Of various types of amphiphilic polymers, poly (maleic anhydride-*alt*-1-octadecene) (denoted as **PMAO**) is favoured because it is cheap, commercially available and has been reported to individually encapsulate such hydrophobic nanocrystals previously [1-2]. In this preliminary study, the MFNPs nanoclusters formability using PMAO were studied to determine the potential use of PMAO and its efficiency to collectively encapsulate MFNPs to form magnetic nanoclusters. Two samples of PMAO-coated magnetic nanoclusters samples (core: MFNPs-2) with different MFNPs loading (using different initial MFNPs concentration of 25 $mg.mL^{-1}$ and 50 $mg.mL^{-1}$), namely MFNCs-P1 (low loading) and MFNCs-P2 (high loading) were successfully fabricated.

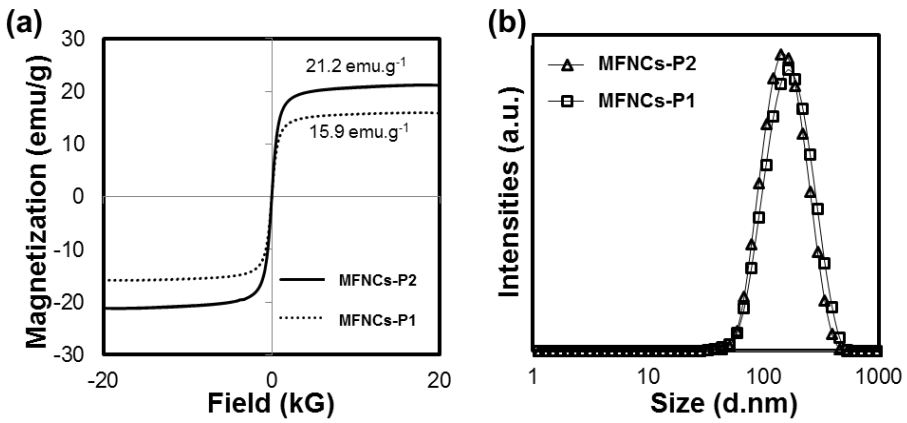

Fig. S4 (a) Hysteresis loop of MFNCs-P_1 and MFNCs-P_2 samples at 300K. (b) Hydrodynamic size distribution of MFNCs-P_1 and MFNCs-P_2 samples in water measured by DLS experiment.

As shown in **Fig.S3**, both MFNCs-P1 and MFNCs-P2 samples were spherical in shape. The VSM results suggested that both MFNCs-P1 and MFNCs-P2 samples still exhibited superparamagnetism, similar to its parents MFNPs-2 core properties (see **Fig S4**). The saturation magnetization (M_S) 15.9 emu.g^{-1} and 21.2 emu.g^{-1} were recorded for MFNCs-P1 (low loading) and MFNCs-P2 (high loading) samples respectively. The dynamic light scattering (DLS) experiments revealed hydrodynamic sizes of 180.2 ± 4.2 and 163.7 ± 3.5 nm for MFNCs-P_1 and MFNCs-P_2 respectively. No secondary peak was observed from the size distribution implying that no severe aggregation was presence in the samples. Overall, the nanoclusters formed by pure PMAO polymers hydrodynamic sizes were rather large, mainly due to the presence of very hydrophobic segments of the PMAO polymers. The high hydrophobicity of PMAO, characterized by its low hydrophilic-lipophilic balance (HLB) value, prevents the emulsion-sonification process to break up the oil phase easily and therefore resulting in a very large cluster sizes. Such large hydrodynamic sizes (≥ 150 nm) were unsuitable for various biomedical applications which might impair the colloidal stability of the formed clusters as demonstrated below.

Colloidal Stability of MFNCs formed by pure PMAO

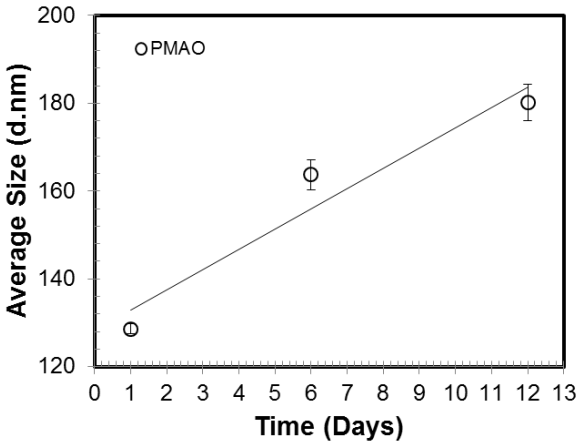

Fig. S5 Hydrodynamic size of nanoclusters formed by PMAO at various incubation time (room temperature).

Nanoclusters formed by PMAO under 12 minutes sonication (as mentioned **Fig. S3** and **Fig. S4**) was relatively large with hydrodynamic size of more than 150 nm. In an attempt to reduce the size of the nanoclusters formed by PMAO, the sonication time was extended during the mini-emulsion/solvent evaporation process. As a results, we obtained a relatively smaller nanoclusters formed by PMAO (128.54 ± 1.2 nm). As shown in the **Fig. S5**, after 6 days and 12 days incubation, the hydrodynamic size of nanoclusters formed by pure PMAO recorded during DLS experiment has increased by approximately ~27% and ~40% from original hydrodynamic size. This kinetic stability study by using DLS showed that these nanoclusters formed by pure PMAO were colloidally unstable and prone to aggregation.

S3. PMAO-g-PEG ^{1}H-NMR Spectra Analysis

The chemical structure of PMAO-g-PEG was further analyzed by ^{1}H-NMR (Bruker DPX300 NMR spectrometer; 300MHz). The chemical shift for PMAO-g-PEG was analyzed by referencing to the solvent peak (δ = 7.24 ppm for Chloroform-d).

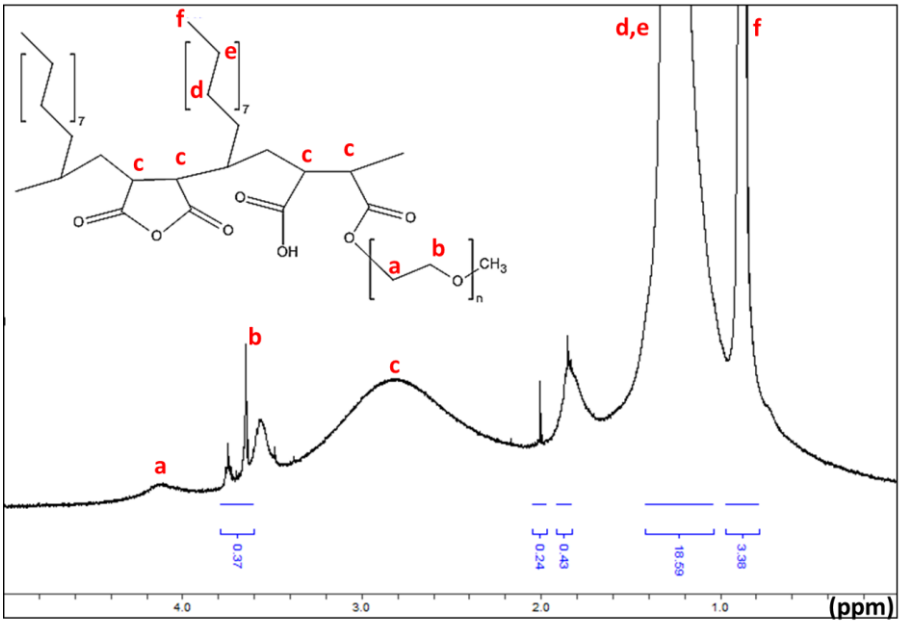

Fig. S6 ^{1}H-NMR spectra of PMAO-g-PEG (solvent: chloroform-d, 300MHz).

From the NMR spectrum (**Fig. S6**), the characteristic peaks due to the resonance of –C$\underline{H}_3$ and –C$\underline{H}_2$ of C_{18} alkyl chain (octadecene) of the hydrophobic section of PMAO were observed around 0.9 ppm and 1.2-1.3 ppm respectively. The acid catalyzed esterification reactions would open the succinic anhydride ring, leaving one carboxylic acid and one ester bond between PMAO and mPEG-OH. The presence of PEG was confirmed by the characteristic chemical shift of the PEG chain at 3.6-3.7 ppm and 4.0-4.25 ppm.

The chemical shifts for PMAO-g-PEG. ^{1}H-NMR (300MHz, $CDCl_3$), δ: 0.9 ppm (f; –CH_2–CH_2–C$\underline{H}_3$), 1.2-1.3 ppm (d,e; –C$\underline{H}_2$–C$\underline{H}_2$–), 2.6-3.2 ppm (c; C–O–C–C$\underline{H}$–C$\underline{H}$–C), 3.6-3.7 ppm (b; O–CH_2–C$\underline{H}_2$–O–CH_3), 4.0-4.25 ppm (a; O–C$\underline{H}_2$–CH_2–O–CH_3), 7.24 ppm ($CDCl_3$ solvent peak, not shown).

S4. Nanoclusters Formability Study: PMAO-g-PEG

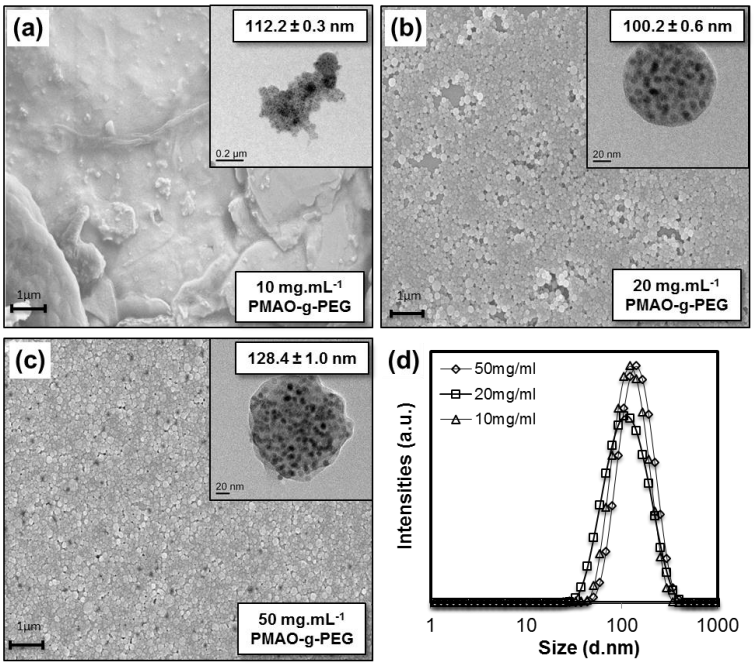

Fig. S7 SEM images of magnetic nanoclusters using PMAO-g-PEG at different concentration (a) 10 mg.mL^{-1}, (b) 20 mg.mL^{-1} and (c) 50 mg.mL^{-1} (insets: TEM images of the respective samples) . (d) Hydrodynamic size of the magnetic nanoclusters prepared using different PMAO-g-PEG in water.

It was predicted that the grafting of PEG functional group towards PMAO could improve the water solubility, improve protein repellent properties (reduce opsonisation) as well as reducing the overall hydrodynamic size during oil-in-water emulsion since its hydrophilic-lipophilic balance (HLB) value would increase. However the grafting of PEG towards PMAO to form PMAO-g-PEG posts a critical question of the correct amount of PMAO-g-PEG to be used to form the magnetic nanoclusters. In this section, 3 different PMAO-g-PEG amounts (concentration) were tested to check the formability of the magnetic nanoclusters (using MFNCs-B2), mainly 10mg, 20mg and 50mg (10mg.mL^{-1}, 20 mg.mL^{-1} and 50 mg.mL^{-1}). From the TEM images of the nanoclusters formed using these three different concentration, 20mg.mL^{-1} was found to be the optimum amount in order to form perfect spherical nanoclusters.

S5. FT-IR of MFNPs and MFNCs

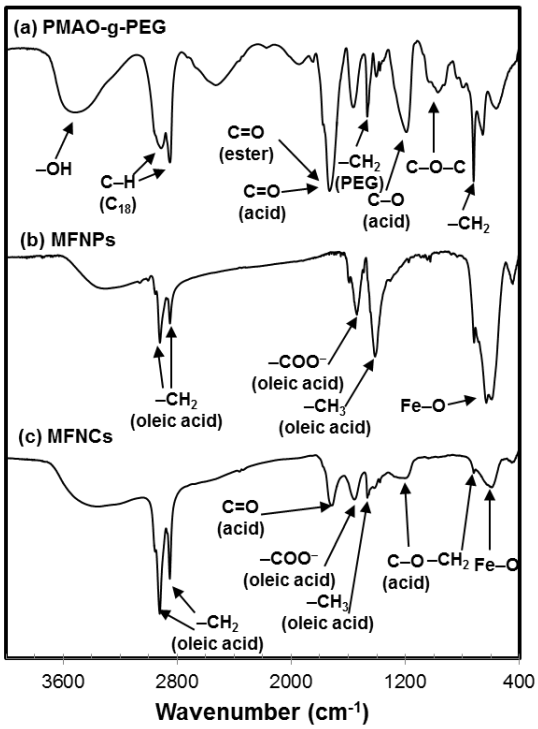

Fig. S8 FT-IR spectra of (a) PMAO-g-PEG, (b) MFNPs and (c) MFNCs.

The main characteristic of hydrophobic MFNPs peaks were observed from the presence of oleic acid capping agent characteristic adsorption peaks. As shown in **Fig. S8b**, Fe–O stretching at around 567 cm^{-1} indicated the bonding between MFNPs and the oxygen containing functional group of oleic acid. The bonding involves the formation of $–COO^–$ group that interacts with Fe atom which verified through the characteristic asymmetric and symmetric stretching vibrations of $–COO^–$ group at 1527 cm^{-1} and 1571 cm^{-1} respectively. The presence of oleic acid alkyl chain was also verified through the existence of asymmetric and symmetric $–CH_2$ vibrations at 2845 cm^{-1} and 2914 cm^{-1} as well as the existence of strong $–CH_3$ bending vibrations at 1399 cm^{-1}. After the formation of MFNCs (from **Fig. S8c**), it can be seen that the carboxylic acid characteristic adsorption peaks from PMAO-g-PEG, mainly C–O and C=O stretching vibrations at 1168 cm^{-1} and 1697 cm^{-1} were presence on top of $–COO^–$ group from oleic acid/Fe atom interactions. The characteristic Fe–O stretching vibrations at 567 cm^{-1} which indicated the presence of MFNPs bonding with oxygen containing functional group of oleic acid. Overall, the FTIR results of MFNCs suggested the presence of MFNPs and PMAO-g-PEG mixture.

S6. Tuning Nanoclusters Core: Further Characterization

The hysteresis loop of MFNCs A-D measured at 300K were shown in **Fig. S9a** and its corresponding thermogravimetric analysis (TGA) results were given in **Fig. S9b**. The TGA results showed that the MFNPs weight fraction in MFNCs samples were around 20-30%.

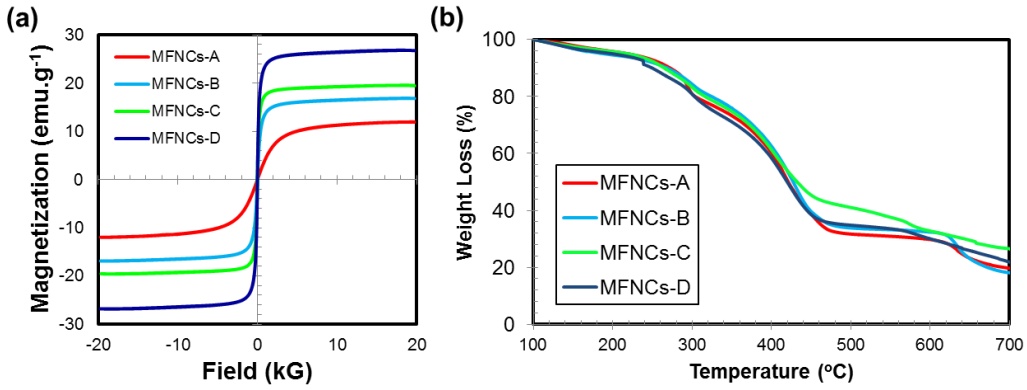

Fig. S9 (a) Hysteresis loop of MFNCs A-D samples measured by VSM experiment at 300K. (b) TGA results of MFNCs A-D samples.

The hydrodynamic sizes, saturation magnetization (M_S) values and its weight fraction of MFNCs A-D with different MFNPs cores size were tabulated in **Table S1** below.

Table S1 Summary of various MFNCs A-D samples with different loading.

Sample	MFNPs Core	d_{hyd} (nm)	M_S (emu.g^{-1})	MFNPs Weight Fraction (%)
MFNCs-A	~6 nm	104.7 ± 1.5	11.93	19.69%
MFNCs-B	~11 nm	106.2 ± 1.1	16.83	19.59%
MFNCs-C	~14 nm	79.2 ± 1.0	19.46	26.54%
MFNCs-D	~18 nm	82.5 ± 0.9	26.75	24.97%

S7. Tuning Nanoclusters Loading: Further Characterization

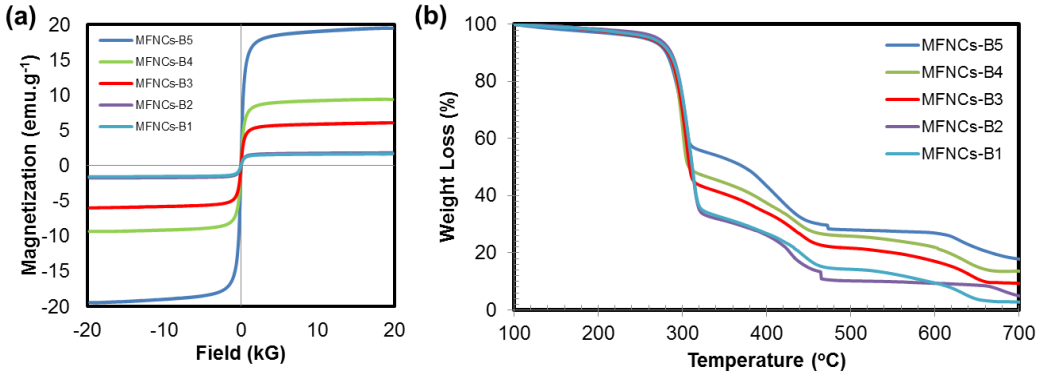

Fig. S10 (a) Hysteresis loop of various MFNCs samples with different loading measured by VSM experiment at 300K. (b) TGA results of various MFNCs samples with different loading.

The hysteresis loop of MFNCs B1-5 measured at 300K were shown in **Fig. S10a** and its corresponding thermogravimetric analysis (TGA) results were given in **Fig. S10b**. The TGA results showed that the MFNPs weight fraction in the MFNCs samples increased with the increase of MFNPs-B loading. The TGA results and magnetization plot against the loading amount agreed closely with the observed MFNPs particles density shown in **Fig. S11** below (assuming perfect spherical nanoclusters).

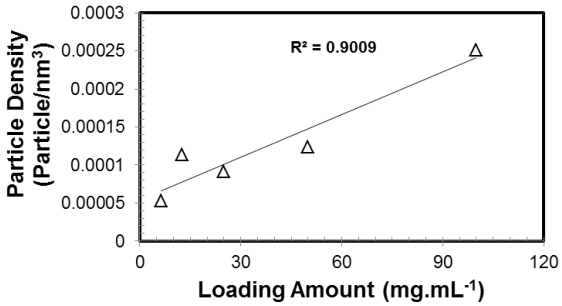

Fig. S11 Plot of the particle density against the initial MFNPs precursor loading amount.

Table S2 Summary of various MFNCs B1-5 samples with different loading.

Samples	MFNPs Amount (mg)	MFNPs/Polymer Mass Ratio	Particle Density (No of Particles/nm^3)	Weight Loss (%)	M_S (emu/g)
MFNCs-B5	20 mg	1.0	25.1 x 10^{-5}	82.08	19.47
MFNCs-B4	10 mg	0.5	12.4 x 10^{-5}	86.39	9.35
MFNCs-B3	5 mg	0.25	9.18 x 10^{-5}	90.64	6.04
MFNCs-B2	2.5 mg	0.125	11.3 x 10^{-5}	94.92	1.78
MFNCs-B1	1.25 mg	0.0625	5.3 x 10^{-5}	96.20	1.62

S8. TEM Average Size and Size Distribution of MFNCs

Table S3 Summary of MFNCs TEM average sizes, DLS hydrodynamic sizes and number of particles per nanoclusters for different MFNCs formulations.

Samples	DLS Average Size	TEM Average Size	No. of Particles per Nanoclusters
PMAO-g-PEG Samples - Core Tuning			
MFNCs-A	104.7 ± 1.5 nm	91.1 ± 12.1 nm	91.3 ± 24.6
MFNCs-B	106.2 ± 1.1 nm	96.0 ± 16.9 nm	58.9 ± 20.1
MFNCs-C	79.2 ± 1.0 nm	52.6 ± 6.1 nm	11.2 ± 3.1
MFNCs-D	82.5 ± 0.9 nm	64.3 ± 14.0 nm	12.6 ± 4.3
PMAO-g-PEG Samples - Loading Tuning			
MFNCs-B1	120.0 ± 0.6 nm	71.4 ± 5.0 nm	14.6 ± 4.0
MFNCs-B2	93.1 ± 0.4 nm	69.0 ± 7.3 nm	17.3 ± 6.5
MFNCs-B3	86.7 ± 0.7 nm	76.1 ± 7.2 nm	25.6 ± 4.6
MFNCs-B4	81.1 ± 1.2 nm	67.0 ± 11.0 nm	38.4 ± 8.7
MFNCs-B5	75.9 ± 0.4 nm	66.5 ± 7.5 nm	48.3 ± 13.4

The average sizes of the nanoclusters measured from TEM were carried out manually by measuring the size of the nanoclusters from both low and high magnification TEM images. Meanwhile, the number of magnetic nanoparticles per nanoclusters was estimated by a simple counting of the total number of magnetic nanoparticles from the nanoclusters TEM images. The sampling size of the measurement was at least 60 nanoclusters. As tabulated in **Table S3**, the TEM average for MFNCs-A, MFNCs-B, MFNCs-C and MFNCs-D (increasing core size) were 91.1 ± 12.1 nm, 96.0 ± 16.9 nm, 52.6 ± 6.1 nm and 64.3 ± 14.0 nm. And the TEM average for MFNCs-B1, MFNCs-B2, MFNCs-B3, MFNCs-B4 and MFNCs-B5 (increasing core loading) were 71.4 ± 5.0 nm, 69.0 ± 7.3 nm, 76.1 ± 7.2 nm, 67.0 ± 11.0 nm and 66.5 ± 7.5 nm. The size distributions of MFNCs nanoclusters with different core size and MFNCs with different loading amount were given in **Fig. S12** and **Fig. S13** respectively. On the other hand, from **Table S3**, it can be observed that the nanoparticles cores size increases or the loading amount decreases (decrease in the MFNPs/PMAO-g-PEG mass ratio), the number of magnetic nanoparticles per nanoclusters decreases.

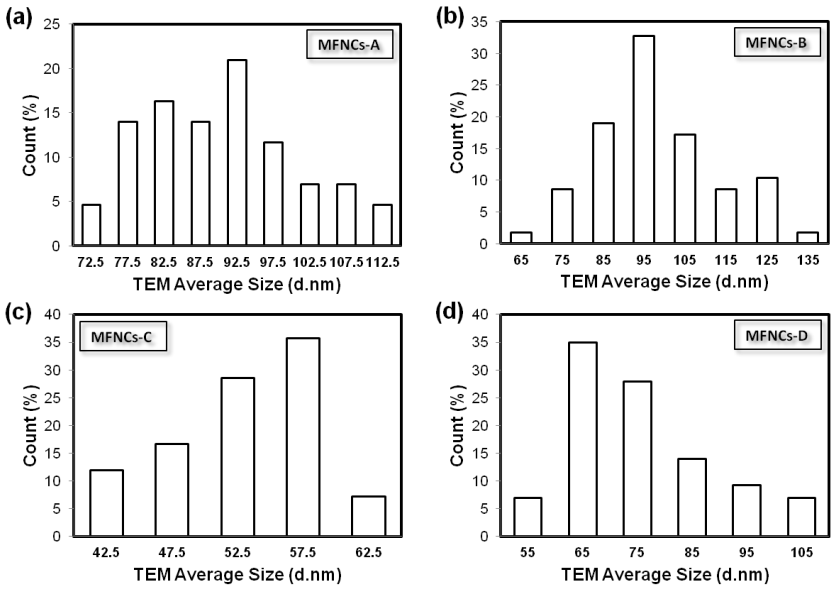

Fig. S12 Nanoclusters TEM average-sizes of: a) MFNCs-A, b) MFNCs-B, c) MFNCs-C, d) MFNCs-D.

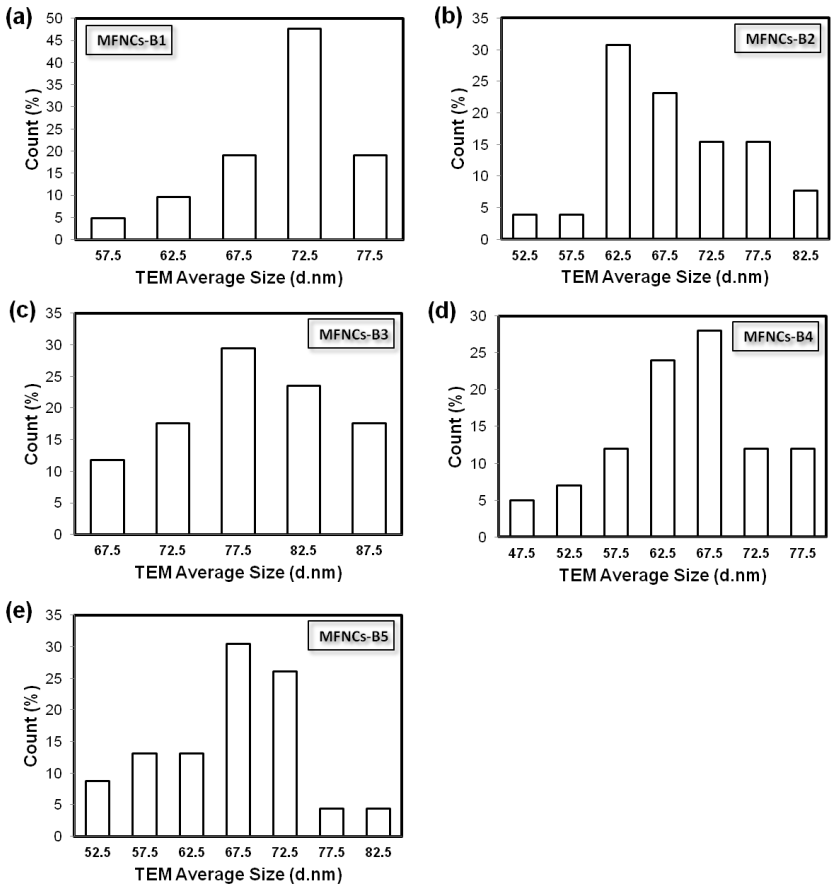

Fig. S13 Nanoclusters TEM average-sizes of: a) MFNCs-B1, b) MFNCs-B2, c) MFNCs-B3, d) MFNCs-B4 and e) MFNCs-B5.

Fig. S14a,b summarized both TEM and DLS average size of nanoclusters samples with different core-size and loading amount. It can be observed that in both cases, the hydrodynamic size of the nanoclusters were always larger than the TEM average size. The discrepancies between the TEM and DLS average size can be explain from the difference in the measurement conditions. During the hydrodynamic size measurement by DLS experiment, these nanoclusters samples were dispersed in aqueous solvent (i.e. water). In this condition, the nanoclusters formed by PMAO-g-PEG would swell during the measurement, especially with the presence of hydrophilic PEG functional group. Therefore, the hydrodynamic size of the nanoclusters (DLS average size) would have to include this swelling and size expansion due to water penetration into the nanoclusters. On the other hand, when these nanoclusters were observed under electron microscope, the nanoclusters were in the dried-state. In this condition, the nanoclusters formed by PMAO-g-PEG would appear much smaller.

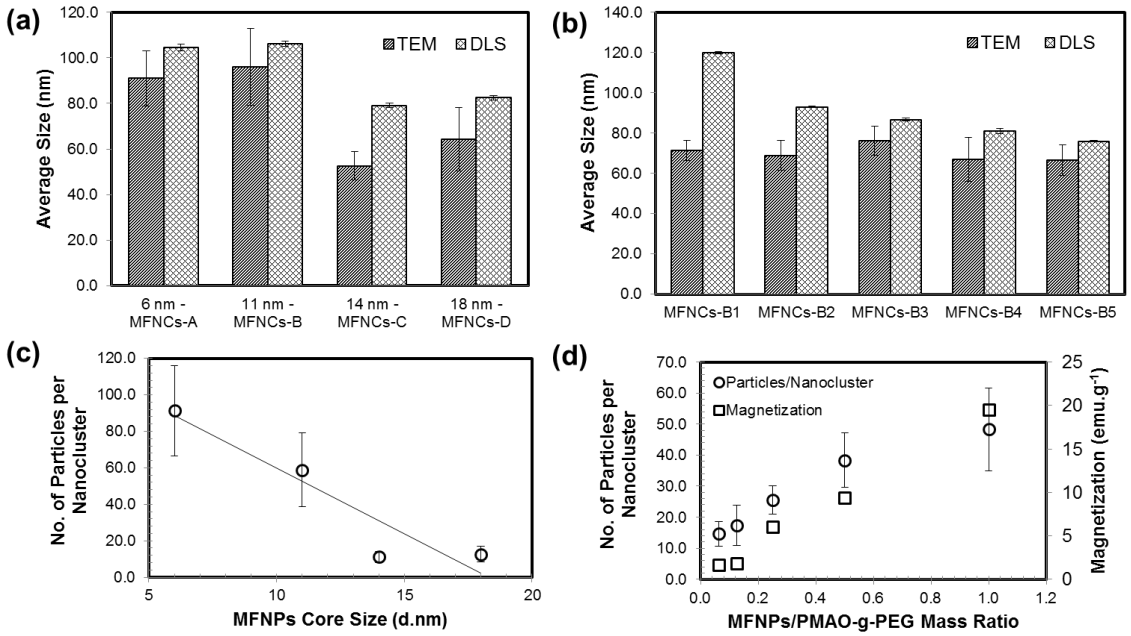

Fig. S14 TEM and DLS average size of nanoclusters with different formulations: (a) core-size and (b) loading amount. Plot of the number of nanoparticles per nanoclusters against (a) MFNPs core size and (b) MFNPs/PMAO-g-PEG mass ratio.

Moreover, in dried-state, the TEM average sizes of the MFNCs-B1 to MFNCs-B5 (as shown in **Fig. S14b**) were relatively the same. The tuning of the nanoclusters loading amount, would barely affect the TEM average size of the nanoclusters. This result significantly demonstrated

that as long as the core size nanoparticles are relatively similar in size, nanoclusters with similar size can be obtained despite the loading amount. Meanwhile, hydrodynamic sizes of MFNCs tend to decrease as loading increases. The decrease in the MFNCs loading is equivalent to the presence of more amphiphilic brush copolymers PMAO-g-PEG amount in the MFNCs (as shown from the TGA results of MFNCs-B1-5 given in the manuscript). As the nanoclusters contained more PMAO-g-PEG, the nanoclusters would swell more in aqueous solvent, resulting in larger hydrodynamic size.

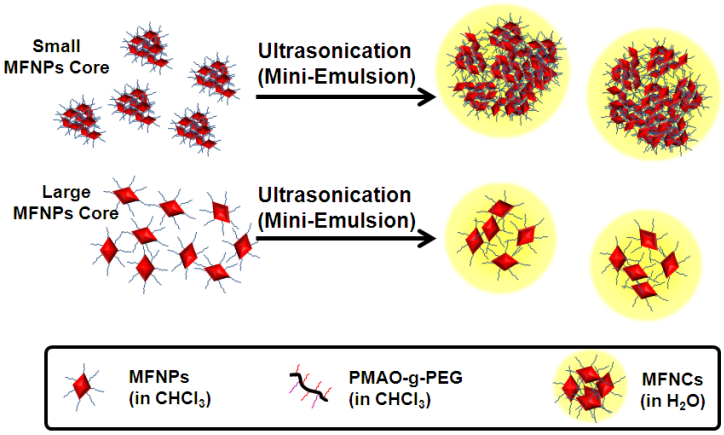

Fig. S15 Schematic of formation of nanoclusters with different MFNPs core sizes.

From **Fig. S14a,** it was observed that the overall nanoclusters diameter decreases with the increasing core size. One plausible explanation was smaller nanoparticles core tends to form aggregate while larger nanoparticles can be easily broken down during the mini-emulsion/solvent evaporation experiment. As illustrated in **Fig. S15**, smaller MFNPs core which possess higher surface energy (due to size effect, high surface-to-volume ratio) would have higher tendency to form small aggregates in order to minimize the total system energy. Thus it is easier for the sonication process during miniemulsion/solvent evaporation to break-down the oil-in-water (O/W) droplet containing PMAO-g-PEG, chloroform and the core nanoparticles to form smaller O/W droplet size if the core nanoparticles size did not aggregate together. As a results, the number of nanoparticles recorded per nanoclusters also decrease as the core nanoparticles increased (as suggested from **Fig. S14c**). It is also possible to control the overall emulsion droplet size, by tuning the sonication time to adjust the energy input to the O/W droplet. In other word, it is possible to maintain the as-synthesized nanoclusters size while changing the core

nanoparticles size, simply by tuning the sonication time. However, extending sonication time would inherently lead to the increase in the samples polydispersity as well as irregularities/inhomogeneity of the nanoclusters morphology [3]. Because of this, the sample morphology irregularities and size polydispersity might vary for different core size formulations despite similar nanoclusters size obtained by adjusting sonication time.

Lastly, **Fig. S14d** suggested that the number of magnetic nanoparticles per nanoclusters is proportional with loading amount of the nanolusters as well as the saturation magnetization values (M_S values).

S8. AIZS Quantum Dots: TEM, HRTEM and XRD Characterization

The size and morphology of orange color emission AIZS quantum dots in chloroform were recorded by TEM as shown in **Fig. S16a**. From the inset of **Fig. S16a**, the HRTEM images of AIZS nanoparticles showed lattice spacing of 0.14 nm which corresponds to (112) plane. The crystalline structure of AIZS nanoparticles was confirmed from its XRD pattern which matches the bulk ZnS and bulk $AgInS_2$, as shown in **Fig. S16b**. The standard XRD patterns ZnS and $AgInS_2$ were given for reference.

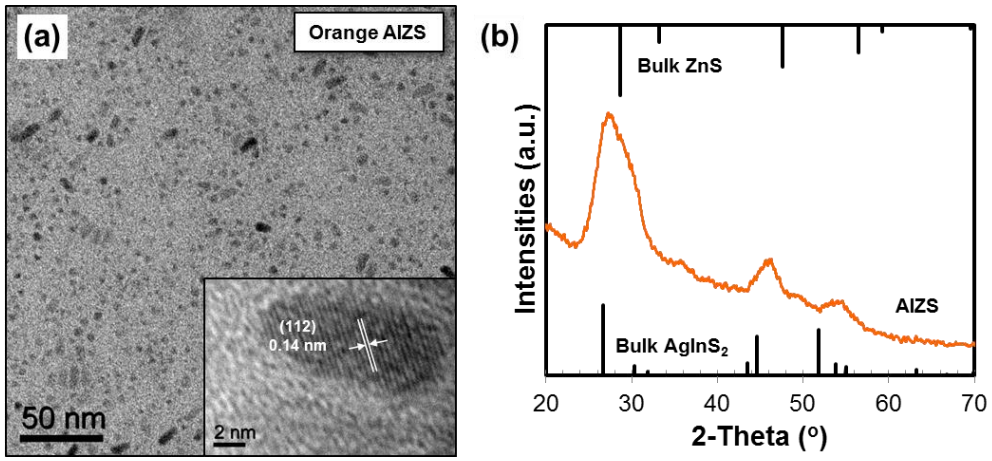

Fig. S16 (a) TEM image of orange color AIZS in chloroform (inset: high resolution TEM image of the respective sample). (b) XRD pattern of the orange color AIZS.

S9. A-MFNCs: VSM, DLS and EDX and Quantum Yield Measurement

VSM, DLS and EDX Characterization:

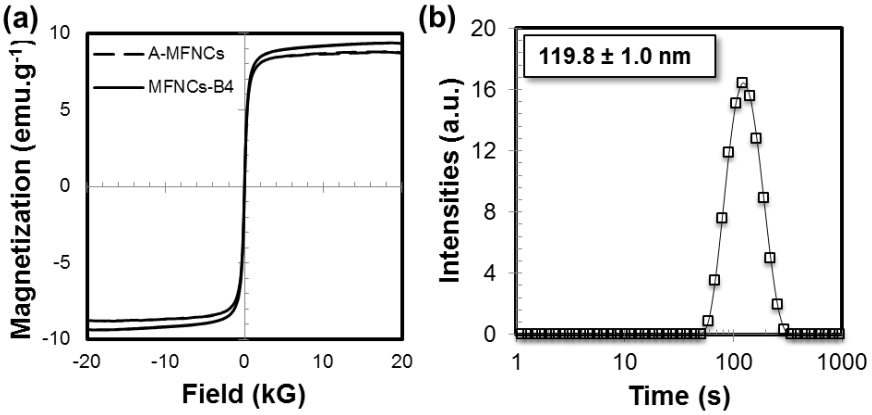

Fig. S17 (a) Hysteresis loop of A-MFNCs measured by VSM experiment at 300K (the hysteresis loop of MFNCs-B4 is also given as a comparison). (b) Hydrodynamic size of A-MFNCs in water measured by DLS experiment at 300K.

As given in **Fig. S17a**, with a similar initial MFNPs precursor amount (same concentration and mass), AIZS QDs loaded MFNCs (A-MFNCs) with M_S value of 8.76 emu.g^{-1} possessed almost similar magnetic properties as compared to MFNCs-B4 (9.35 emu.g^{-1}). From **Fig. S17b**, the hydrodynamic was found to be 119.8 ± 1.0 nm.

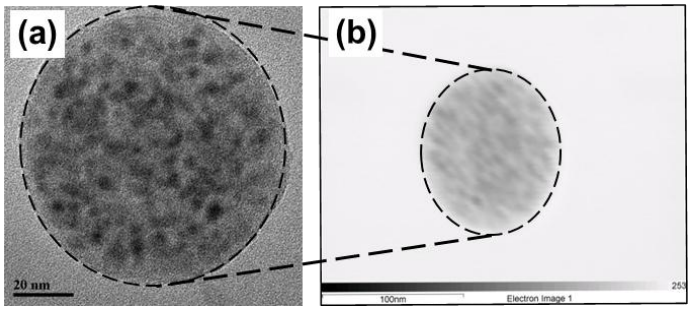

Fig. S18 (a) Original A-MFNCs high magnification TEM image, (b) Actual position of A-MFNCs during the mapping process.

To confirm the presence of all the 6 elements in MFNCs, TEM EDX mapping were carried out to spatially quantify the presence of Fe, Mn, Ag, In, Zn and lastly S. The TEM and the actual position of the A-MFNCs sample used in the TEM EDX mapping were given in **Fig. S18**.

Element	Weight%	Atomic%
Fe K	10.60	6.68
Mn K	1.50	0.97
O K	27.23	60.05
Ag L	25.56	8.33
In L	13.26	4.05
Zn K	7.26	3.88
S K	14.59	16.04

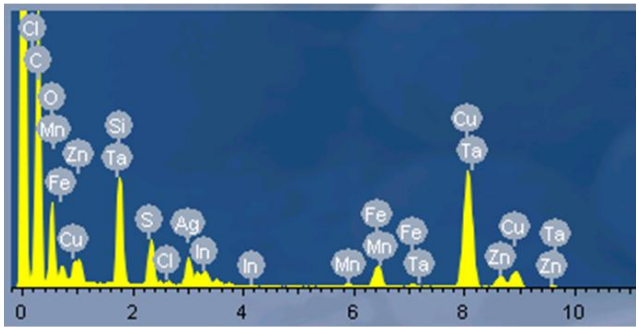

Fig. S19 EDX spectrum of A-MFNCs and its elemental analysis.

The overall EDX elemental quantification analysis shown in **Fig. S19** revealed a breakdown of 6.68 at% Fe, 0.97at% Mn, 8.33 at% Ag, 4.05 at% In, 3.88 at% Zn and 16.04 at% S. The atomic ratio between Mn and Fe indicated that Mn was actually doped onto Fe_3O_4 structures.

Quantum Yield Measurement:

To investigate the quenching of fluorescence quantum dots after the formation of multifunctional nanoclusters, the fluorescence quantum yield (QY) of the samples was measured. QY describes the ratio of photons absorbed to photons emitted through the fluorescence. The QYs of the samples were measured as follow [4]:

$$QY = QY_{st}\frac{F_{samples}}{F_{st}}\cdot\frac{f_{st}}{f_{samples}}\cdot\left(\frac{n_{samples}}{n_{st}}\right)^2 \quad (1)$$

Where F is the spectrally integrated photon flux measured (area under the emission spectrum which has been corrected for blank emission), f is the absorption factor and lastly n is the refractive index. In all measurement, rhodamine 101 dye in ethanol (literature quantum yield QY_{st} = 100%) with emission range of 600-650 nm that is close to the emission of orange AIZS was used as standard materials [5].

Table S4 Summary of various MFNCs A-D samples with different loading.

Samples	Solvent	Z-Average	Emission (nm)	QYs
QDs	Hexane	-	634	35%
A-MFNCs	Water	119.8 nm	610	13.73%

As summarized in **Table S4**, the QYs of orange AIZS (emission range: 634 nm) in hexane was around 35%. When orange AIZS embedded together with MFNPs-B to form A-MFNCs, the overall QY decreases to 13.7%. The decrease in the QY of A-MFNCs as compared to the original AIZS in hexane can be due to various factors. For instance, (1) during the sonication in the mini-emulsion/solvent evaporation process, the surface of the orange AIZS were slightly oxidized. Such reduction in the QY due to the sonication has been also previously reported by our group whereby more than 40% QY reduction was obtained when orange AIZS samples were dispersed in water with the presence of graphene oxide [6]. (2) The absorption of visible wavelength by MFNPs-core and amphiphilic brush copolymers PMAO-g-PEG would also lead to the decrease in the amount of visible wavelength absorbed by the orange AIZS.

With the excess of fluorescence AIZS in the multifunctional nanoclusters, the contribution from the magnetic nanoparticles core would diminish. As such, the MR relaxivity performance as MRI T_2 contrast agent would be deteriorated. On the other hand, when the amount of fluorescence AIZS was reduced, the fluorescence signals from the nanoclusters would diminish, and the QY would be negligible. Therefore during the preparation of multifunctional nanoclusters, the balance of the mass-ratio between the AIZS and MFNPs core must be maintained.

S10. TEM EDX Mapping of MFNCs-B2

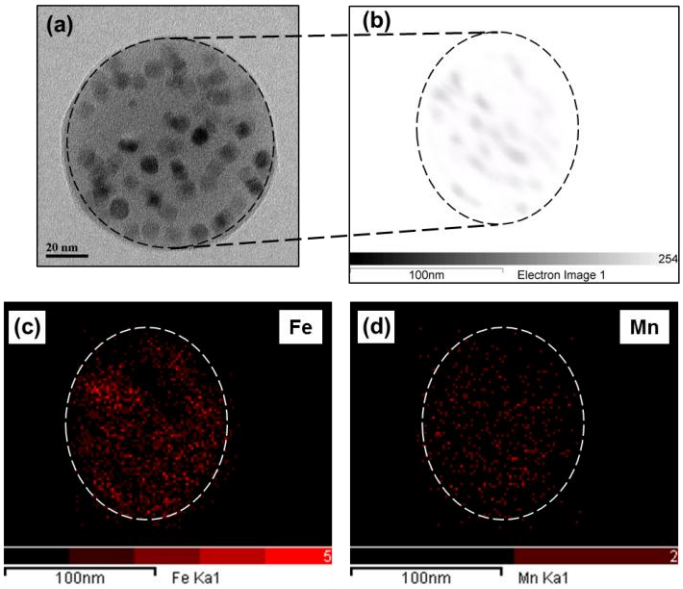

Fig. S20 TEM EDX elemental mapping of MFNCs-B2: (a) original high magnification TEM image of MFNCs-B2, (b) actual position of MFNCs-B2 during the mapping process. 2 elements were mapped, mainly (c) Iron (Fe), (d) Manganese (Mn).

From the MFNCs-B2 EDX mapping shown in **Fig. S20**, the presence of $MnFe_2O_4$ magnetic nanoparticles (MFNPs) were confirmed with the presence of Mn and Fe elements. The overall EDX elemental quantification analysis shown in **Fig. S21** revealed a breakdown of 75.25 at% Fe, 4.77 at% Mn. The atomic ratio between Mn and Fe indicated that Mn was actually doped onto Fe_3O_4 structures.

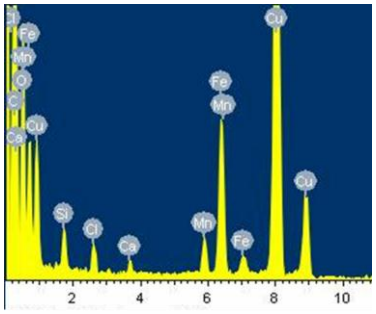

Element	Weight%	Atomic%
Fe K	46.63	75.25
Mn K	10.19	4.77
O K	43.18	19.98

Fig. S21 EDX spectrum of MFNCs-B2 and its elemental analysis..

S11. CLSM Image: High Magnification and Stacking

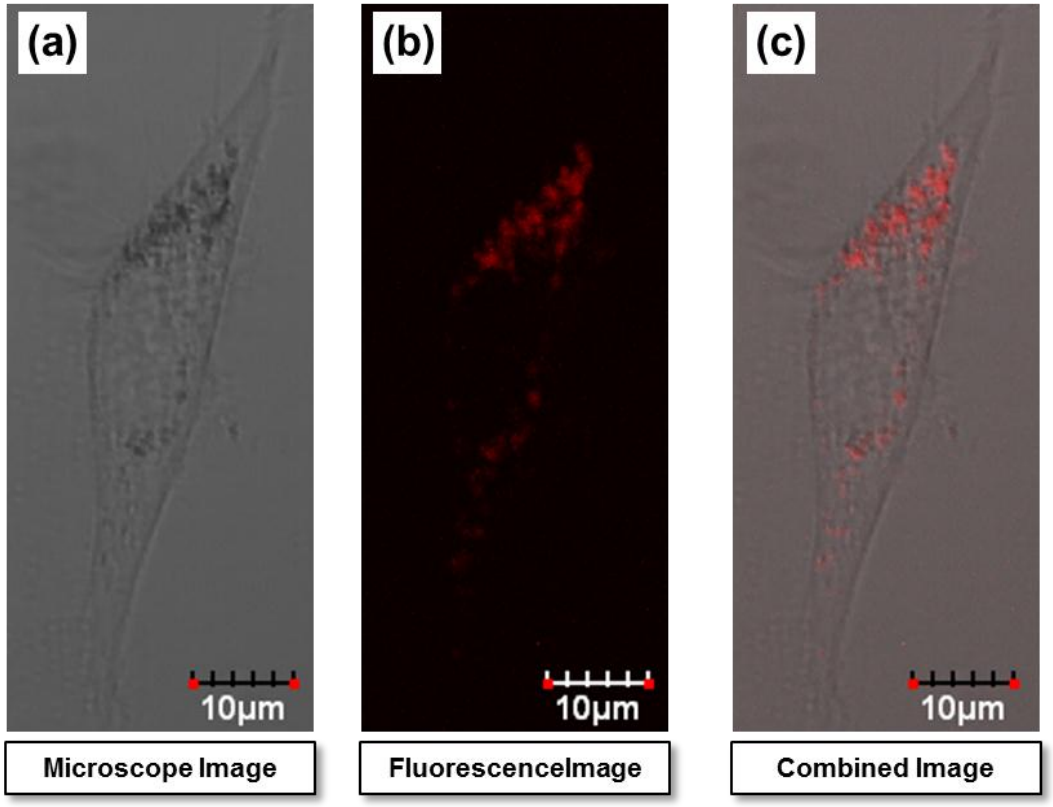

Fig. S22 High magnification CLSM image of NIH/3T3 cells incubated with A-MFNCs: (a) Microscope image, (b) Fluorescence image and (c) Combined image. From the combined image, A-MFNCs were clearly found to reside inside the cell cytoplasm.

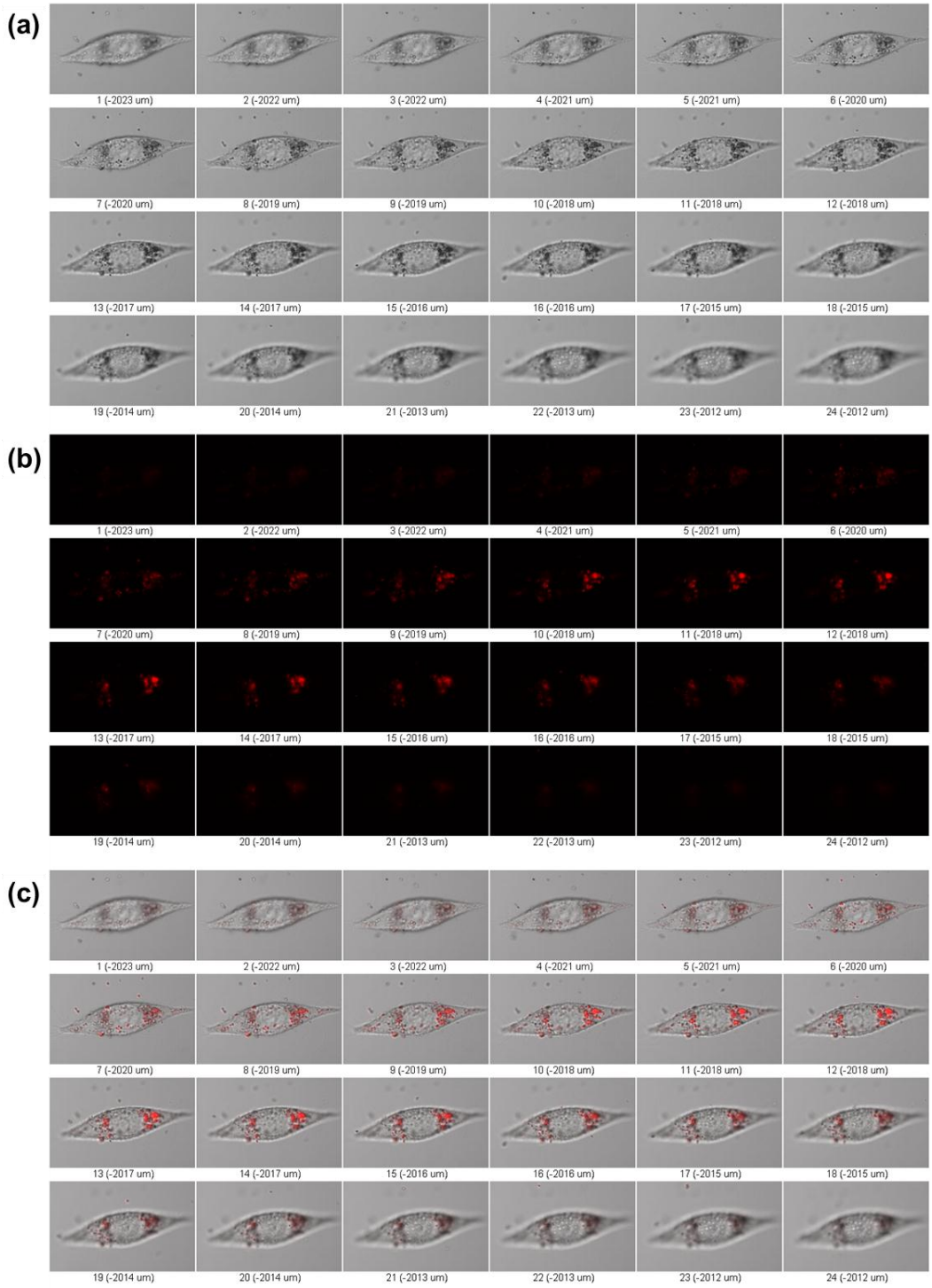

Fig. S23 CLSM image of NIH/3T3 cell incubated with A-MFNCs: (a) microscope image, (b) fluorescence image and (c) combined image at different z-depth that were used to construct the 3D stacking images of NIH/3T3 cell.

S12. Elemental Analysis of MFNCs and Cell Cytotoxicity of MFNCs Formed by Pure PMAO

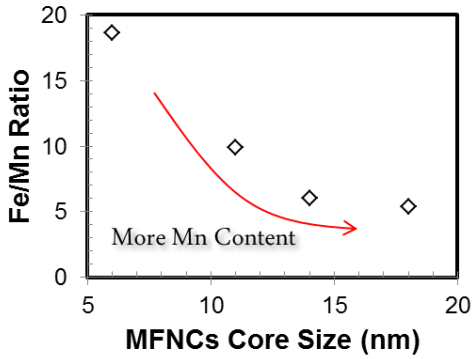

Fig. S24 Elemental analysis results of MFNCs samples with different MFNPs core size (using inductively coupled plasma optical emission spetrosopy).

MFNCs-D loaded with largest MFNPs core (MFNPs-D; ~18nm) was chosen to be evaluated in the cell cytotoxicity study because of (1) its high saturation magnetization of the MFNPs core. Higher saturation magnetization samples would normally prone to severe/more aggregation during cell studies. If the non-specific aggregation occurs, this larger aggregate of nanoclusters would bring more harm to the NIH/3T3 cells [7-8]. Moreover, the presence of the manganese in the MFNCs might induce severe neurotoxicity [9]. The elemental analysis of various MFNCs samples containing different MFNPs core size shown in **Fig. S24** below revealed that MFNCs-D which was loaded with MFNPs-D appears to have significantly lower Fe/Mn atomic ratio (more manganese content). Based on these two reasons, samples MFNCs-D was chosen for cell biocompatibility test in NIH/3T3 cells.

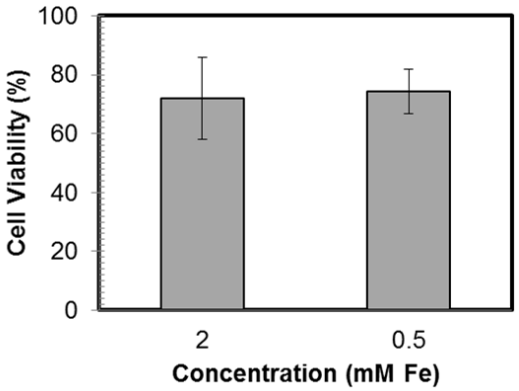

Fig. S25 Cell cytotoxicity of PMAO-coated MFNCs (core: MFNPs-D).

The biocompatibility of the nanoclusters formed by PMAO (without the presence of PEG) using MFNPs-D core were assessed by incubating the samples with NIH/3T3 mouse fibroblast cells for 24 hours prior to the cytotoxicity assay using CCK-8. From the *in-vitro* cytotoxicity results given in **Fig. S25** above, nanoclusters formed by PMAO at 0.5 mM and 2.0 mM iron concentration induced more than 20% cell death after 24 hours incubation. In comparison with MFNCs-D samples (**Fig. 8b**) which showed cell viability of more than 96.8% at 1.75 mM iron concentration, nanoclusters formed by pure PMAO was less biocompatible as compared to the nanoclusters formed by PMAO-g-PEG.

Reference

[1]. W. Y. William, C. Emmanuel, M. S. Christie, D. Rebekah and L. C. Vicki, *Nanotechnology*, 2006, **17**, 4483.

[2]. L. M. Bronstein, E. V. Shtykova, A. Malyutin, J. C. Dyke, E. Gunn, X. Gao, B. Stein, P. V. Konarev, B. Dragnea and D. I. Svergun, *The Journal of Physical Chemistry C*, 2010, **114**, 21900-21907.

[3]. R. H. Staff, D. Schaeffel, A. Turshatov, D. Donadio, H.-J. Butt, K. Landfester, K. Koynov and D. Crespy, *Small*, 2013. (DOI: 10.1002/smll.201300372)

[4]. M. Grabolle, M. Spieles, V. Lesnyak, N. Gaponik, A. Eychmüller and U. Resch-Genger, *Anal. Chem.*, 2009, **81**, 6285-6294.

[5]. T. Karstens and K. Kobs, *J. Phys. Chem.*, 1980, **84**, 1871-1872.

[6]. Y. Sheng, X. Tang, E. Peng and J. Xue, *J. Mater. Chem.*, 2013, **1**, 512-521.

[7]. S. L. Saville, R. C. Woodward, M. J. House, A. Tokarev, J. Hammers, B. Qi, J. Shaw, M. Saunders, R. R. Varsani, T. G. St Pierre and O. T. Mefford, *Nanoscale*, 2013, **5**, 2152-2163.

[8]. J.-E. Bae, M.-I. Huh, B.-K. Ryu, J.-Y. Do, S.-U. Jin, M.-J. Moon, J.-C. Jung, Y. Chang, E. Kim, S.-G. Chi, G.-H. Le e and K.-S. Chae, *Biomaterials*, 2011, **32**, 9401-9414.

[9]. D. E. McMillan, *Neurotoxicology*, **20**, 499-507.